Liquid Spreading

Deutsche Ausgabe: DOI: 10.1002/ange.201607514
Internationale Ausgabe: DOI: 10.1002/anie.201607514

Uni-Directional Transportation on Peristome-Mimetic Surfaces for Completely Wetting Liquids

Chuxin Li[+], Ning Li[+], Xinshi Zhang, Zhichao Dong, Huawei Chen,* and Lei Jiang*

Abstract: *Liquid uni-directional transport on solid surface without energy input would advance a variety of applications, such as in bio-fluidic devices, self-lubrication, and high-resolution printing. Inspired by the liquid uni-directional transportation on the peristome surface of Nepenthes alata, here, we fabricated a peristome-mimicking surface through high-resolution stereo-lithography and demonstrated the detailed uni-directional transportation mechanism from a micro-scaled view visualized through X-ray microscopy. Significantly, an overflow-controlled liquid uni-directional transportation mechanism is proposed and demonstrated. Unlike the canonical predictions for completely wetting liquids spreading symmetrically on a high-energy surface, liquids with varied surface tensions and viscosities can spontaneously propagate in a single preferred direction and pin in all others. The fundamental understanding gained from this robust system enabled us to tailor advanced micro-computerized tomography scanning and stereo-lithography fabrication to mimic natural creatures and construct a wide variety of fluidic machines out of traditional materials.*

A lively topic for centuries is the quest for directional transportation of liquids without using an external force. Biological surfaces, such as the back of desert beetles,[1] spider silk,[2] butterfly wings,[3] cacti,[4] bird beaks,[5] and the peristome of pitcher plant,[6] harness their micro-scaled morphologies or wettabilities to control liquid transportation for survival. By mimicking these surfaces, several strategies have been proposed to induce preferential liquid motion, including chemical modification,[7] hetero-wettability fabrication,[8] and directional motion through chemical reactions,[9] temperature differences,[10] and geometrical effects.[11] Directional movements of liquids induced by the unbalanced surface tension forces constitute an important surface phenomenon,[12] and understanding the physicochemical mechanisms could help develop new liquid transportation devices.[2,5] However, several drawbacks still exist and limit practical usage: 1) The amplitude of liquid motion is limited to the size of the drop as well as the gradient on the surface.[4] 2) Liquid motion must often be triggered by injecting energy into the system, using light,[13] vibrations,[5] or heat,[14] because the resulting capillary force is comparable to the sticking force that induced by defects on the solid. 3) The left–right symmetry of the anisotropic wetting property on grooved structures limits its transportation ability.[15] If these problems were properly solved, directional liquid transportation would be of great value in diverse applications,[16] such as fog collection,[10] high-resolution printing,[17] lubrication,[6] and micro-fluidic operations.[18]

Herein, inspired by the spontaneously uni-directional transportation mechanism on the peristome surface of *Nepenthes alata*,[6] we mimic the surface morphology of the peristome surface through high-resolution stereo-lithography to fabricate microcavity-arrayed substrates with varied surface energies. Owing to the stereo-lithography fabrication method, sophisticated structures can be fabricated on demand. We harness the structure of peristome surface to achieve uni-directional liquid transportation without external energy input. Unlike the canonical predictions for low surface tension liquids spreading symmetrically on a high-energy surface,[19] liquids with varied surface tensions and viscosities can propagate in a single preferred direction and pin in all others. Significantly, the complexly wetting liquid, FC-72 (perfluorohexane), with a surface tension of 9.5 $mN\,m^{-1}$, can spontaneously and uni-directionally spread on the peristome-mimetic surface. The micro-scaled overflow or anti-overflow behavior on the peristome-mimetic surface is visualized and demonstrated with X-ray microscopy, where overflow-controlled liquid uni-directional spreading mechanism is proposed. Through experiments and modelling, the uni-directional transportation characteristic was quantified, depending on the surface morphologies of the fabricated surface, surface-wetting properties, liquid surface tension, and viscosity.

In our experiments, we constructed peristome-mimetic surfaces using high-resolution stereo-lithography. To modify the substrates with varied surface energies, the fabricated substrates were oxygen-plasma-treated for different durations to hydroxylate the surface with high surface energies, as well as fluorinated to achieve low surface energies. The substrate was then mounted on the platform with two high-speed cameras capturing the flow dynamics from vertical and horizontal directions. Viscous and non-viscous droplets were

[*] C. Li,[+] N. Li,[+] X. Zhang, Dr. Z. Dong, Prof. L. Jiang
Key Laboratory of Bio-inspired Smart Interface Sciences
Technical Institute of Physics and Chemistry
Chinese Academy of Sciences
Zhongguancun East Road, 29, 100190, Beijing (P.R. China)
E-mail: dongzhichao@iccas.ac.cn
C. Li,[+] N. Li[+]
School of Chemistry and Engineering
University of Chinese Academy of Sciences
Yuquan Road, 100049, Beijing (P.R. China)
Prof. H. Chen
School of Mechanical Engineering and Automation
Beihang University
Beijing 100191 (China)
E-mail: chenhw75@buaa.edu.cn
[+] These authors contributed equally to this work.

Supporting information for this article can be found under: http://dx.doi.org/10.1002/anie.201607514.

 © 2016 Wiley-VCH Verlag GmbH & Co. KGaA, Weinheim

individually or consequently dispensed though a micro-syringe pump onto the fabricated surface. Liquids with surface tensions ranging from 9.5 to 72.0 mN m^{-1}, and viscosity ranging from 0.3 to 96.0 mPs were utilized to investigate the influence of surface tension as well as the viscosity on liquid uni-directional transportation.

Figure 1 a–c shows the morphologies of the peristome-mimetic surface, the cliv-entrapped and arch-shaped micro-cavities arrayed surface (CAMAS). According to the spreading abilities, the arched microcavities, with a typical length of 700 μm, a width of 250 μm and a depth of 150 μm, are regularly aligned along the axial direction with periodic overlapped configuration. Titled and cross-sectional SEM views show that the cavities slightly slanted into the surface at an angle of ≈20° with a closed apex in front and a sharped overhang structure at rear. High-magnification images showed that the radius of curvature (RoC) is 75 μm at the apex, while less than 1 μm at the rear (Figure 1 c). Such a shaped overhang structure is assumed to resist motion of the liquid at the rear side,[20] while the deposited liquid directionally spreads toward the top of the microcavity (Figure 1 d and e).

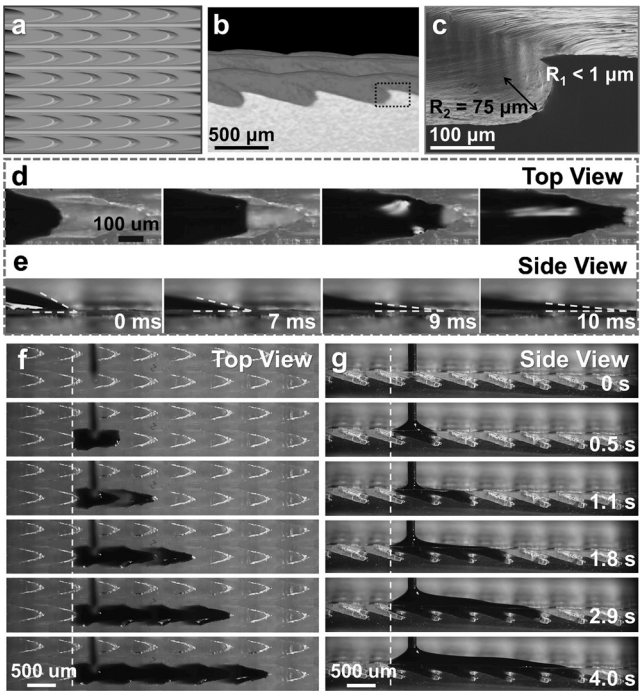

Figure 1. Liquid uni-directional transportation on peristome-mimic surface. a) Image of the peristome-mimetic surface fabricated by computer-aided design. b, c) Cross-sectional micro-CT and scanning electron microscope (SEM) images of the fabricated surface, respectively. c) A sharp overhang at the rear side of the arch-shaped microcavity with a curvature of less than 1.0 μm, which can reduce the liquid overflow at the rear side. d–g) Time-lapse images of uni-directional spreading of a water droplet and continually deposited liquid. d, e) In situ observation of dyed water uni-directional transportation on a peristome-mimetic surface. A water droplet (dyed by Indian ink) is dropped onto the surface through a capillary tube with a superamphiphobic opening. The deposited water (20.0 μL) can uni-directionally transport in a single microcavity with an average velocity of 50.0 mm s^{-1}. f, g) Through continual liquid deposition, dyed water could uni-directionally spread in a single direction and pin in all of the others.

Time-lapse images of Figure 1 f and g show that water uni-directionally spread along arrayed microcavities without retraction when dyed water, Indian ink, was continually deposited onto the CAMAS. The precursor advanced first at an accelerating speed toward the apex of cavities, then, slowed at the apex. After a brief stagnant period, the liquid precursor elevated and overflowed the micro-overhang. As a result, it propagated toward the apex of the next arched microcavity with an accelerating speed. In contrast to the liquid bi-directional transportation on channel-featured films, the deposited liquid cannot overflow the barrier at the rear side of the CAMAS,[21] but can uni-directionally spread in a single preferred direction (Figure S1).

In addition to water uni-directionally spreading on a hydrophilic surface, water can also spontaneously spread on the CAMAS with varied wettabilities (Figure 2 a, Figure S2 and Movie S1). The threshold contact angle θ_t for uni-directional spreading was 64.4°, similar to the newly defined critical angle, 65°.[22]

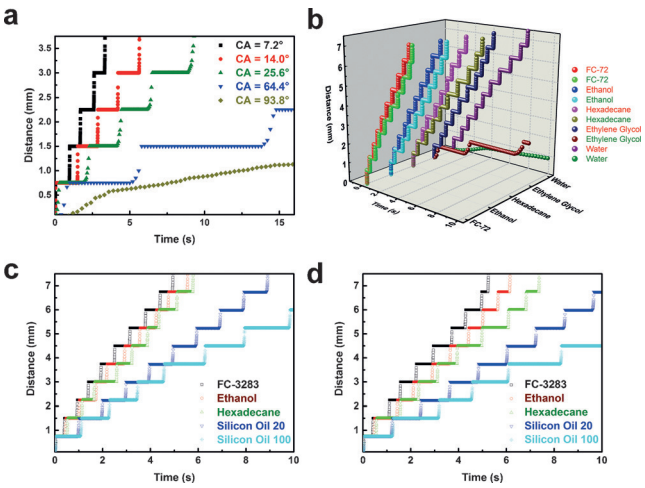

Figure 2. Time sequences of the uni-directional transporting distances. a) 20.0 μL water directional transportation on peristome-mimetic surfaces with varied wettabilities. The squares, circles, and triangles show impulsive growth with uni-directional liquid transportation, and crosses (the bottom line) show the experimental results, which are nearly uni-directional transportation with liquid propagation, respectively. (Detailed animations can be seen in Movie S1). The threshold contact angle θ_t for uni-directional transportation is 64.4°. b) Non-viscous liquids (20.0 μL) with surface tensions ranging from 9.5 to 72.0 mN m^{-1} can uni-directionally transport on the hydrophilic (red characters) and hydrophobic (green characters) CAMAS spontaneously. FC-72, the completely wetting liquid with lowest surface tension, could still uni-directionally transport on the CAMAS with the fastest speed. Detailed images and data can be seen in Figure S2. c, d) Viscous liquids with viscosities between 0.3 to 96.0 mP spread on the CAMAS with hydrophilicity (c) and hydrophobicity (d). For almost all of the non-viscous liquids and viscous liquids that can be ejected from the dispensing nozzle, uni-directional liquid transportation can be achieved without further energy input (Figures S3–S6). The slope of the curve indicates the flow velocity. Flow velocity increases with increasing surface energy, decreasing liquid surface tension, and reducing liquid viscosity.

© 2016 Wiley-VCH Verlag GmbH & Co. KGaA, Weinheim

In contrast to previous reports that simply focused on the motion of water, here, other liquids with complete wetting properties (for example, ethanol and acetone; Figures S3 and S4) and high viscosities (ethylene glycol, hexadecane, and silicon oil; Figures S5 and S6) were also investigated and showed uni-directional transportation on the CAMAS (The physical and chemical properties of these tested liquids can be found in the Table S1,S2 in Supporting Information). Notably, FC-72, the lowest surface-tension liquid,[20a] could also achieve uni-directional transportation. Time sequences of 20.0 μL of the liquid transporting distances with varied surface tensions are shown in Figure 2b, and varied viscosities in Figure 2c, d.

The impulse-typed plots observed on the curves of Figure 2 can be explained as followings: The microcavity allows continuous and inward liquid transportation, and the speed of liquid spreading along or filling the microcavity accelerates as the precursor approaching the apex of the cavity. After the liquid layer fills up a microcavity, the hysteresis effect induced by the curvature differences between the top of the cavity and the overhang structure plays a major obstacle for liquid motion, introducing an impulse-typed liquid transportation style.

To help understand the mechanism of overflow-controlled liquid uni-directional transportation, we utilized micro-computerized tomography (micro-CT) to demonstrate the liquid–solid wetting state in a 3D view (Movie S2). Ethylene glycol (EG) with a surface tension of 48.2 $mN\,m^{-1}$ and a viscosity of 16.1 mPs was deposited onto the vertically mounted CAMAS with the opening of the microcavities down. The wetting state is captured at a resolution of 1.0 μm and shown in Figure 3. The upper liquid exceeds and overflows the overhang as well as fills up the upper microcavity (the transition from S1 to S2 in Figure 3c). Whereas, the liquid–solid contact line still pins in place and follows the outline of sharped overhangs (Figure 3b), though gravity acts to drag the EG overflowing the rear-side of the microcavity. Because of the energy barrier at the rear side,[23] even 2.0 μL EG would not overflow the overhang. In addition, micro-CT images captured at tilted, rotated, and flipped angles clearly demonstrated the morphology of liquid wetting state (Movie S2). The sharped overhang structure thus plays a major role in preventing liquid from spreading in the reverse direction.

Having shown the micro-scaled wetting state of the EG drop on CAMAS and demonstrated the overflow-controlled liquid uni-directional transportation, we next analyzed the driving mechanism for liquid transportation at the precursor. The possible propulsive force for uni-directional liquid spreading could arise from the specific geometries of arched cavities. As shown in Figure 3c,d, the curvature variation of menisci at the overhang and apex gave rise to a difference in Laplace pressure, ΔP, acting on the liquid:[24]

$$\Delta P \approx \frac{\gamma\cos\theta_a}{\alpha x} - - \frac{\gamma\cos\theta_r}{\alpha(x + L)} \quad (1)$$

where γ is the liquid surface tension, θ_a is the contact angle (CA) of the precursor, θ_r is the CA at the rear side, α is the apex angle, x is the distance of the precursor from the apex,

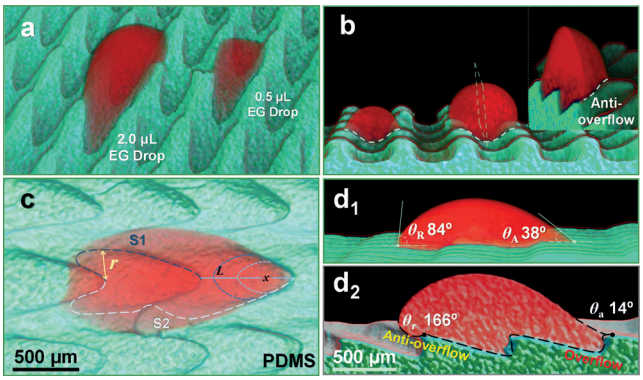

Figure 3. Three-dimensional illustration of the liquid wetting state during the uni-directional spreading process. a) 2.0 μL and 0.5 μL ethylene glycol (EG) deposited on the peristome-mimetic surface vertically mounted on the sample stage with the opening of microcavity down. The images have been color-coded and rotated by the software. b) EG pins at the rear-side of the overhang. Because of the sharp edge, liquid cannot overflow the overhang. c) From S1 to S2, upper liquid exceeds and overflows around the sharp overhang as well as fills up the upper microcavity, whereas, liquid spreading in the reverse direction or vertical directions do not occur. The liquid–solid contact line pins in place and follows the outline of the microcavities. d) Side view (d_1) and cross-section view (d_2) of the advancing and receding contact angles of the liquid on the surface, respectively. Animated video of the 3D wetting state is shown in Movie S2.

and L is the length of precursor, respectively. Because Laplace pressure on the precursor with a small radius of curvature (RoC) is larger than that on the overhang with a large RoC, the resultant pressure gradient over the liquid would drive the precursor towards the apex.[25]

The geometry of microcavities also influences the surface micro-scaled wetting property. The cross section of a liquid drop on CAMAS has unequal contact angles at the precursor side and rear side. As illustrated in Figure $3d_2$, the CA at precursor is 14°, while a large CA of 166° at the overhang, the values of which are quite different from what has been measured by conversional method (Figure $3d_1$). From the micro-CT observations,[26] we could clearly observe the wetting state in detail. A large θ_r on such a shaped overhang is believed to prevent liquid from downward overflow.[20] For the lowest surface tension liquid FC-72, θ_r is undoubtedly below the threshold value to overflow the overhang,[20a] thus ensuring the uni-directional spreading behavior for all nearly non-viscous liquids.

For non-viscous liquids, such as water, methanol, ethanol, and acetone, contact angle hysteresis was previously regarded as a resistant force for liquid motion.[5] The capillary resistant force is scaled as:

$$dFc = \gamma\Delta\cos\theta dx \quad (2)$$

where $\Delta\cos\theta = \cos\theta_R - \cos\theta_A$, θ_R is the receding CA at the precursor, θ_A is the advancing CA at the rear, and dx is the thickness of the section of the drop.[27] However, an interesting phenomenon is observed in Figure 2b, where completely wetting liquids can uni-directionally spread along the CAMAS. This phenomenon can be explained as follows:

© 2016 Wiley-VCH Verlag GmbH & Co. KGaA, Weinheim

the CA at the precursor site is quite smaller than that at the rear side, and CA differences constitute a driving force for liquid movement. Because of the energy barrier induced by the overhang, this combination of Laplace force F_d and capillary hysteresis could permit continually deposited liquid to move uni-directionally.

Unlike water, viscous liquid typically shows a wetting state because of its low surface tension. Resistant force is thus typically provided by its viscosity.[5] A theoretical analysis was performed to infer the spreading velocity at the microcavity, considering that a tiny amount of liquid has a value of $\approx \alpha L^2 \sin\theta_A$, and the pressure drop between these two menisci could scale as $\gamma\cos\theta_a/(\alpha x)$. The corresponding Laplace pressure gradient, $\gamma\cos\theta_a/(\alpha x L)$, over this volume finally yields a capillary driving force varying as

$$F_d \approx \frac{\gamma L^2 \sin\theta_A \cos\theta_a}{x} \quad (3)$$

It can be clearly seen from Equation (3) that F_d increases as the precursor approaches the apex. The fast spreading of continuous liquid flow could therefore be achieved through integrating optimized apex geometry.

When a liquid with a dynamic viscosity η uni-directional spreading at a speed v, the viscous force, F_η, whose magnitude scales as $\eta v L \sin\theta_A/\alpha$, could act and resist liquid spreading. Balancing the propulsive Laplace force and the resistant viscous force, the velocity v can be inferred as:

$$v \approx \frac{\alpha\gamma L\cos\theta_a}{\eta x} \quad (4)$$

The surface tension, viscosity, morphologies, micro-scaled wetting properties are therefore crucial roles to determine the liquid uni-directional transportation. From Equation (4), we can clearly explain the question of why liquid spreads slowly on a hydrophobic surface (Figures S4, S6): For a given liquid with a set value of γ/η, a smaller spreading velocity v is produced on a confined surface (α) with a larger advancing contact angle θ_a.

When continually adding liquid onto the CAMAS, the deposit drops could spread rapidly along the surface with velocities on the order of a few meters per second. This was an interesting phenomenon because the average moving speed of one liquid drop with a volume of 2.0 μL deposited on the surface typically scales as $\approx 50\ \mathrm{mm\,s^{-1}}$. If continually adding liquid onto the wetted surface, the following liquid drops with an even smaller volume of 0.5 μL that impact on the liquid film could attain velocities that are two orders of magnitude higher than the first one. This kind of drop motion could be explained by a loss of interfacial resistance that was introduced by a hydrodynamical lubricating liquid film on the surface. If we can harness this interesting liquid transportation phenomenon, we can directionally transport liquid with less energy loss.

After the fundamental demonstration of our artificial uni-directional spreading system, we then explored several liquid transportation applications by building three-dimensional elevated spiral and two dimensionally fluidic machines through stereo-lithography (Figure 4). Unlike the downward water flow direction of the fountain of *Cologne Cathedral*, water can "climb" along the track of an *Archimedes* spiral and elevate to a height of 10.0 mm. We noted that, because the water layer at the rear side cannot overflow the overhang structures, the liquid–solid contact line at the rear side is unaffected by prior trajectories and is able to withstand the hydrostatic pressure. Within one minute, dyed water could flow along the trajectory with a distance of 45.0 cm, which is a significant speed without an external energy input (Movie S1). Other liquids, such as hexadecane, also flow along the track of the *Archimedes* spiral without flowing in the reverse direction. The CAMAS system is therefore a good candidate in liquid uni-directional manipulation.

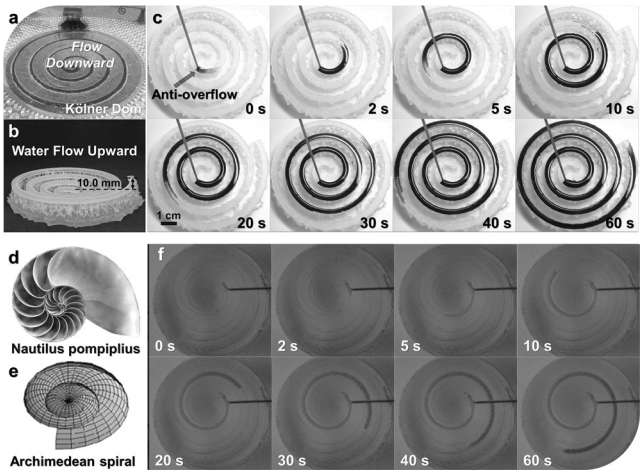

Figure 4. Liquid uni-directional transportation on elevated spiral and Archimedean spiral surfaces. a) Optical images depicting the fountain of Cologne Cathedral. Deposited liquid could flow downward along the spiral. b) Side view of the elevated spiral. Through stereo-lithography, an elevated spiral was fabricated with an elevation of 10.0 mm. c) Continuously depositing dyed water (3.0 mL) onto the center of the spiral, water flows upward and climbs along the curve without retraction at the rear side. Within a minute, dyed water flows a distance of 45 cm and elevates 1 cm. d) Optical images depicting the morphology of *Nautilus pompiplius*, and e) the *Archimedean* spiral designed by computer-aided design (CAD). f) Red-dyed hexadecane (150 μL) can spread along the *Archimedean* spiral without retraction and follow the pattern without expansion.

In summary, we have presented a facile method for mimicking biological surfaces with sophisticated structures through micro-CT observations and high-resolution stereo-lithography. The micro-scaled wetting state of liquid uni-directional transportation process have been visualized through X-ray microscopy, and overflow-controlled uni-directional transportation mechanism has been demonstrated. Even for completely wetting liquids, uni-directional transportation could still be achieved. Our results suggest an innovative bio-mimetic material fabrication method that should find practical applications in liquid transportation control, particularly in the field of fog collection, high-resolution printing, self-lubrication, and micro-fluidic operations.

 © 2016 Wiley-VCH Verlag GmbH & Co. KGaA, Weinheim

Acknowledgements

We acknowledge project funding provided by the National Research Fund for Fundamental Key Projects (2012CB934100, 2013CB933000), the National Natural Science Foundation (21503245, 21421061) and the Key Research Program of the Chinese Academy of Sciences (KJZD-EW-M01).

Keywords: bio-mimetic · computerized tomography · directional transportation · viscous liquids · wetting liquids

How to cite: *Angew. Chem. Int. Ed.* **2016**, *55*, 14988–14992
Angew. Chem. **2016**, *128*, 15212–15216

[1] A. R. Parker, C. R. Lawrence, *Nature* **2001**, *414*, 33–34.
[2] Y. M. Zheng, H. Bai, Z. B. Huang, X. L. Tian, F. Q. Nie, Y. Zhao, J. Zhai, L. Jiang, *Nature* **2010**, *463*, 640–643.
[3] C. C. Liu, J. Ju, Y. M. Zheng, L. Jiang, *ACS Nano* **2014**, *8*, 1321–1329.
[4] J. Ju, H. Bai, Y. M. Zheng, T. Y. Zhao, R. C. Fang, L. Jiang, *Nat. Commun.* **2012**, *3*, 1247.
[5] M. Prakash, D. Quere, J. W. M. Bush, *Science* **2008**, *320*, 931–934.
[6] H. W. Chen, P. F. Zhang, L. W. Zhang, H. L. L. Iu, Y. Jiang, D. Y. Zhang, Z. W. Han, L. Jiang, *Nature* **2016**, *532*, 85–89.
[7] a) N. Ballav, A. Shaporenko, A. Terfort, M. Zharnikov, *Adv. Mater.* **2007**, *19*, 998–1000; b) A. Dupuis, J. Leopoldes, D. G. Bucknall, J. M. Yeomans, *Appl. Phys. Lett.* **2005**, *87*, 024103.; c) M. K. Chaudhury, G. M. Whitesides, *Science* **1992**, *256*, 1539–1541; d) S. Daniel, M. K. Chaudhury, J. C. Chen, *Science* **2001**, *291*, 633–636.
[8] J. Y. Chung, J. P. Youngblood, C. M. Stafford, *Soft Matter* **2007**, *3*, 1163–1169.
[9] X. Yao, H. Bai, J. Ju, D. Zhou, J. Li, H. Zhang, B. Yang, L. Jiang, *Soft Matter* **2012**, *8*, 5988–5991.
[10] K. C. Park, P. Kim, A. Grinthal, N. He, D. Fox, J. C. Weaver, J. Aizenberg, *Nature* **2016**, *531*, 78–82.
[11] X. Heng, C. Luo, *Langmuir* **2015**, *31*, 2743–2748.
[12] N. J. Cira, A. Benusiglio, M. Prakash, *Nature* **2015**, *519*, 446–450.
[13] K. Ichimura, S. K. Oh, M. Nakagawa, *Science* **2000**, *288*, 1624–1626.
[14] a) G. Dupeux, M. Le Merrer, G. Lagubeau, C. Clanet, S. Hardt, D. Quere, *Epl-Europhys. Lett.* **2011**, *96*, 58001; b) G. Lagubeau, M. Le Merrer, C. Clanet, D. Quere, *Nat. Phys.* **2011**, *7*, 395–398.
[15] a) H. Kusumaatmaja, R. J. Vrancken, C. W. M. Bastiaansen, J. M. Yeomans, *Langmuir* **2008**, *24*, 7299–7308; b) R. Seemann, M. Brinkmann, E. J. Kramer, F. F. Lange, R. Lipowsky, *Proc. Natl. Acad. Sci. USA* **2005**, *102*, 1848–1852.
[16] K. H. Chu, R. Xiao, E. N. Wang, *Nat. Mater.* **2010**, *9*, 413–417.
[17] J. Z. Wang, Z. H. Zheng, H. W. Li, W. T. S. Huck, H. Sirringhaus, *Nat. Mater.* **2004**, *3*, 171–176.
[18] a) M. X. Zhang, L. Wang, Y. P. Hou, W. W. Shi, S. L. Feng, Y. M. Zheng, *Adv. Mater.* **2015**, *27*, 5057–5062; b) S. L. Feng, S. J. Wang, L. C. Gao, G. J. Li, Y. P. Hou, Y. M. Zheng, *Angew. Chem. Int. Ed.* **2014**, *53*, 6163–6167; *Angew. Chem.* **2014**, *126*, 6277–6281.
[19] Y. K. Lai, J. Y. Huang, Z. Q. Cui, M. Z. Ge, K. Q. Zhang, Z. Chen, L. F. Chi, *Small* **2016**, *12*, 2203–2224.
[20] a) T. Y. Liu, C. J. Kim, *Science* **2014**, *346*, 1096–1100; b) A. Tuteja, W. Choi, M. L. Ma, J. M. Mabry, S. A. Mazzella, G. C. Rutledge, G. H. McKinley, R. E. Cohen, *Science* **2007**, *318*, 1618–1622.
[21] Z. C. Dong, L. Wu, J. F. Wang, J. Ma, L. Jiang, *Adv. Mater.* **2015**, *27*, 1745–1750.
[22] Y. Tian, L. Jiang, *Nat. Mater.* **2013**, *12*, 291–292.
[23] Z. C. Dong, L. Wu, N. Li, J. Ma, L. Jiang, *ACS Nano* **2015**, *9*, 6595–6602.
[24] P.-G. De Gennes, F. Brochard-Wyart, D. Quéré, *Capillarity and wetting phenomena: drops, bubbles, pearls, waves*, Springer Science & Business Media, Amsterdam, **2013**.
[25] A. Ponomarenko, D. Quere, C. Clanet, *J. Fluid Mech.* **2011**, *666*, 146–154.
[26] a) S. J. Park, B. M. Weon, J. S. Lee, J. Lee, J. Kim, J. H. Je, *Nat. Commun.* **2014**, *5*, 1–7; b) J. S. Lee, S. J. Park, J. H. Lee, B. M. Weon, K. Fezzaa, J. H. Je, *Nat. Commun.* **2015**, *6*, 1–8 .
[27] D. Quéré, *Annu. Rev. Mater. Res.* **2008**, *38*, 71–99.

Received: August 3, 2016
Revised: September 7, 2016
Published online: September 21, 2016

 © 2016 Wiley-VCH Verlag GmbH & Co. KGaA, Weinheim